

Supporting Information

Conductance and assembly of quasi-1D coordination chain molecular junctions with triazole derivatives

Zelin Miao,^a Xiaoyun Pan,^b and Maria Kamenetska^{a,b,c*}

^a *Division of Materials Science and Engineering, Boston University, Boston, Massachusetts,
02215, United States*

^b *Department of Chemistry, Boston University, Boston, Massachusetts, 02215, United States*

^c *Department of Physics, Boston University, Boston, Massachusetts, 02215, United States*

E-mail: mkamenet@bu.edu

Contents

1. Experimental and Calculation Details	S2
2. Additional Conductance Data	S5
3. Additional Calculation Data	S10
4. Reference	S18

1. Experimental and Calculation Details

Scanning Tunneling Microscope-based Break-Junction (STMBJ) Method

Room-temperature conductance measurements are performed under ambient conditions using a home-built STMBJ instrument, as established previously.^{1,2} The substrates are prepared by thermally evaporating a thin layer of Au (> 100 nm, Thermo Scientific Chemicals, 99.9985% metal basis) onto the mechanically polished AFM/STM discs (Ted Pella) using a thermal evaporator (Auto 306 Turbo, Edwards) and annealed with blowtorch prior to use. A freshly cut Au tip (diameter = 0.25 mm; Alfa Aesar, 99.999% metal basis) is pushed into substrate to make metallic contact (conductance > 5 G_0 , where $G_0 = 2e^2/h$). The junction is then retracted at a speed of 20 nm/s for 5 nm, controlled by the single(z)-axis piezoelectric actuator, during which the electric current across the junction and relative displacement of electrodes are recorded (acquisition rate = 40 kHz) under a constant bias (100 mV or 500 mV). During stretching, the junction gradually thins out with reduced Au atoms in the junction cross-section and then ruptures, displaying the plateaus at around multiple integers of G_0 in individual conductance traces, followed by the abrupt drop of conductance to the noise floor. We measure the clean Au a thousand times to make sure the quantum point contact can be achieved, and the surface is free from contamination. Once the point contact breaks, and in the presence of molecules, the nanogap may be bridged by the molecule to form the single-molecule junction, resulting in additional plateau lower than 1 G_0 . We repeat such measurement thousands of times (> 4000) and compile the resulting conductance-displacement traces into logarithmically binned 1D conductance histograms and 2D conductance-displacement histograms without data selection to enable the extraction of the most probable conductance associated with molecules through Gaussian fitting and the geometries that junction can sustain upon elongation, respectively. We measure the conductance of molecules by adding drops of diluted solutions (~1 mM) in organic solvents including *N,N*-dimethylformamide (DMF, Sigma-Aldrich, anhydrous, 99.8%) and 1,2,4-trichlorobenzene (TCB, Sigma-Aldrich, anhydrous, ≥ 99%), or through dip-coating method out of aqueous solutions (1~5 mM) which will be illustrated in detail below. Wax (Apiezon)-coated tip is used to measure the molecule in polar solvent, such as DMF, to suppress the Faradaic background current.^{3,4}

Dip-Coating Sample Preparation from Aqueous Solutions

We prepare the samples using the dip-coating method with the established protocols.⁵⁻⁷ The target molecules are dissolved in nuclease-free water (Sigma-Aldrich, molecular biology reagent) to make 1~5 mM solutions, where pH is adjusted by adding 0.1 M sodium hydroxide (NaOH, Sigma-Aldrich, $\geq 98\%$, pellets) solution or 1.0 N hydrochloric acid (HCl, Sigma-Aldrich) and monitored by pH meter (FiveEasy F20, Mettler Toledo). The Au-coated substrates that have been tested free from contamination are immersed in the solution for 20 minutes, and then oven-dried (Digital Gravity, Quincy Lab) with temperature no higher than 65 °C. It should be noted that the indicated pH pertains to the aqueous solution before evaporating the solvent and the pH values reported here are within ± 0.5 . We demonstrate in **Figure S1** the comparison between the dip-coating method and the results obtained from the solution-based measurement using wax-coated tips for 1,2,4-triazole (Tr124) at pH 9. Though both methods show similar conductance signatures, the low noise-to-signal ratio prevents us from resolving the high-G peaks in solution. We therefore use the dip-coating method to measure conductance of molecules from aqueous environments in this work.

Experimental Error

To assess experimental error, we rely on standard error definition:

$$e_G = \frac{\Delta G}{\sqrt{N}}$$

where ΔG is the standard deviation of conductance and N is the number of measurements. Each histogram presented here contains ~ 10000 (no fewer than 4000) traces, so $\sqrt{N} \approx 100$. To estimate the error, we observe from our data that $\Delta G \sim G_{mean}$, where G_{mean} is the most probable value of conductance, assuming a Gaussian distribution. In other words, for a peak centered at $10^{-2} G_0$, the width of the peak $\Delta G \sim 10^{-2} G_0$. We conclude that the error, $e_G \approx 0.01 G_{mean}$ or 1% of the peak position.

Density Functional Theory (DFT)-based Calculations

Transmission calculations of metal-molecule-metal junctions are performed using DFT-based nonequilibrium Green's functions (NEGF) implemented in AITRASS postprocessing package within FHI-aims,⁸⁻¹⁰ with the Perdew-Burke-Ernzerhof (PBE) functional for exchange-

correlation.¹¹ We use ‘tight’ level basis set (double-zeta basis set plus polarization equivalent) for atoms in molecules and ‘loose’ basis set (double-zeta basis set equivalent) for Au atoms in electrodes, respectively.¹² We initially optimize the geometry of molecules (including chain structures in **Figure 5** and **Figure S14**) and then append two Au18 pyramids to the potential binding sites (nitrogen atoms) of the molecule to form Au-N bonds. Each molecule is relaxed with two electrodes while constraining the positions of the back two layers of gold atoms until all force components per atom within the junction are lower than 10^{-2} eV/Å. We vary the Au-N bond distance on each side by a small length step (0.05 Å) to search the junction geometries with the total energy minima. Interaction forces (binding energy) are calculated through subtracting the energy of each component (two electrodes and molecule) from the total energy of the relaxed junction structure. We use the combination of two dull Au21 electrodes or one sharp Au22 and one dull Au21 electrode to calculate the N-Au bond strength of anionic Tr124⁻ when considering all three nitrogen atoms binding to Au (**Figure S12**). Transmission spectra as function of energy at zero bias are calculated then using NEGF embedded in AITRASS package. Gas-phase frontier molecular orbitals (MOs) of neutral and anionic triazole isomers are calculated using FHI-aims with a ‘tight’ level basis set and are plotted using the same contour value of 0.1.

2. Additional Conductance Data

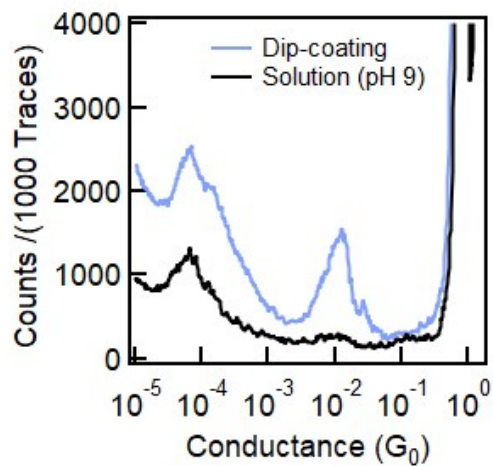


Figure S1. 1D conductance histograms of Tr124 obtained via dip-coating method or in solution using wax-coated tips at pH 9 and aqueous environments ($V_{\text{bias}}=100$ mV). This condition is obtained after dissolving Tr124 molecules into water without any pH adjustments. Both dried and aqueous conditions yield the same molecular conductance values, but the lower signal-to-noise for high-G signature is observed in solution-based measurement.

We plot the conductance histograms of Tr123 measured out of water with pH 2 and 8, in addition to pH 12 in **Figure S2**, with the overlaid histogram obtained from DMF solution (**Figure 2**). We observe a π - π stacking junction signature in acidic conditions (pH 2) as indicated by a peak at $\sim 10^{-3} G_0$. Furthermore, we ascribe the high-G peaks associated with pH 8 and pH 12 aqueous conditions to the junctions formed with an anionic version of Tr123, although the low-G chain signature can only be resolved at the extremely basic condition (pH 12). More importantly, we find that the high-G peak from DMF solution with fitted conductance of $1.31 \times 10^{-2} G_0$ is slightly lower than that from the basic aqueous condition. We exclude solvent effects by showing almost identical conductance values of Tr124 measured in DMF solution and pH 9 aqueous condition in the main text (**Figure 3**). Measurements of Tr123 with various pH conditions under 100 mV and 500 mV show no obvious bias-dependent behaviors, as indicated in **Figure S4**.

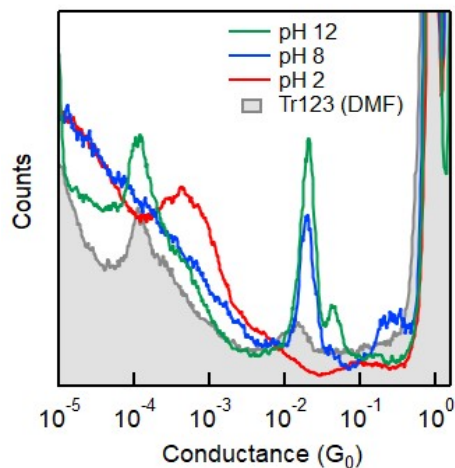


Figure S2. Overlaid conductance histograms of Tr123 dip-coated on gold from aqueous solutions with varying pH (2, 8, and 12) compiled from 5000 individual traces. Dissolving molecules in water results in a solution with pH 8. Histogram of Tr124 measured in DMF solution from **Figure 2a** is reproduced here for comparison.

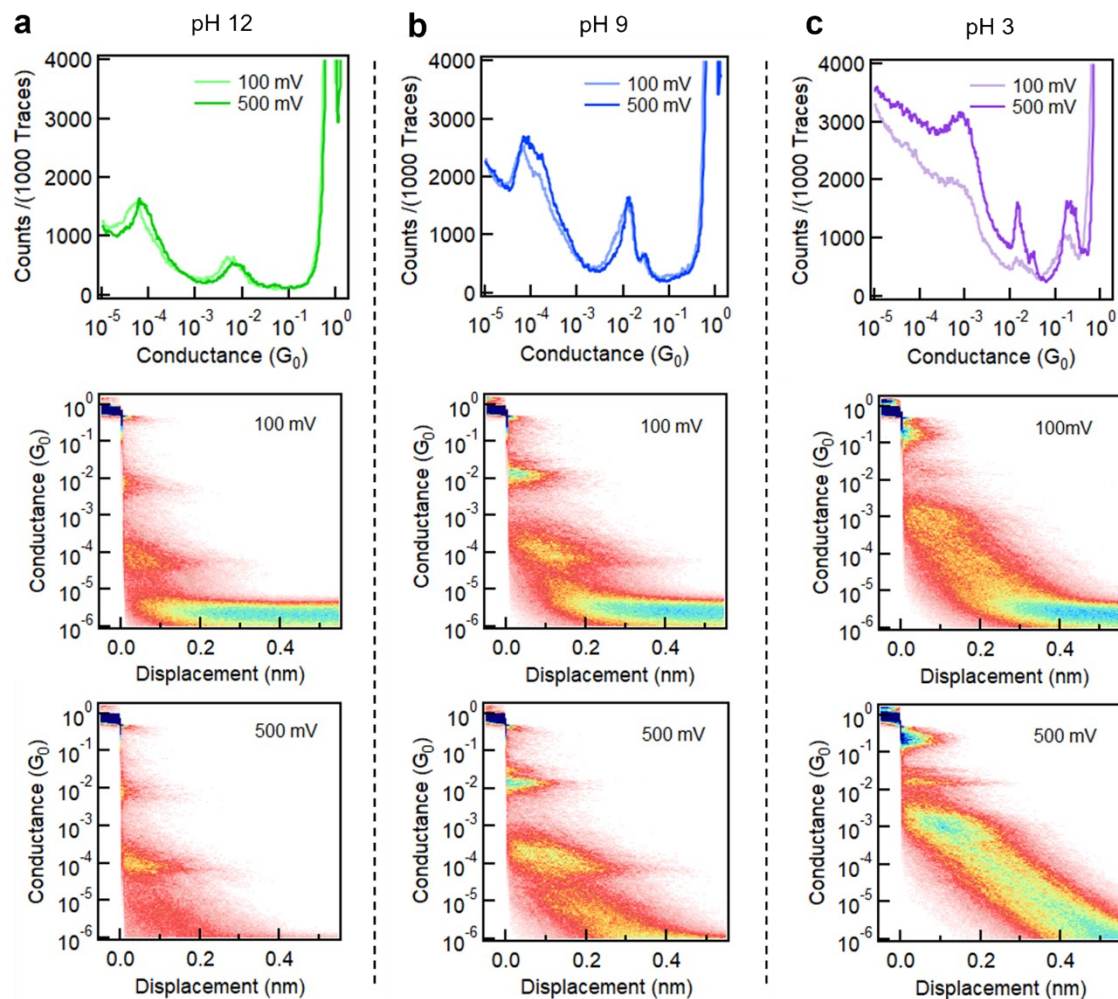


Figure S3. 1D and 2D conductance histograms of Tr124 measured out of various aqueous conditions: **(a)** pH 12, **(b)** pH 9, and **(c)** pH 3 with low ($V_{\text{bias}}=100$ mV) and high ($V_{\text{bias}}=500$ mV) applied voltages using the dip-coating method. No apparent voltage-induced conductance shift is observed for all conditions. We also observe the increased counts of conductance signatures at pH 3 collected at 500 mV compared to 100 mV.

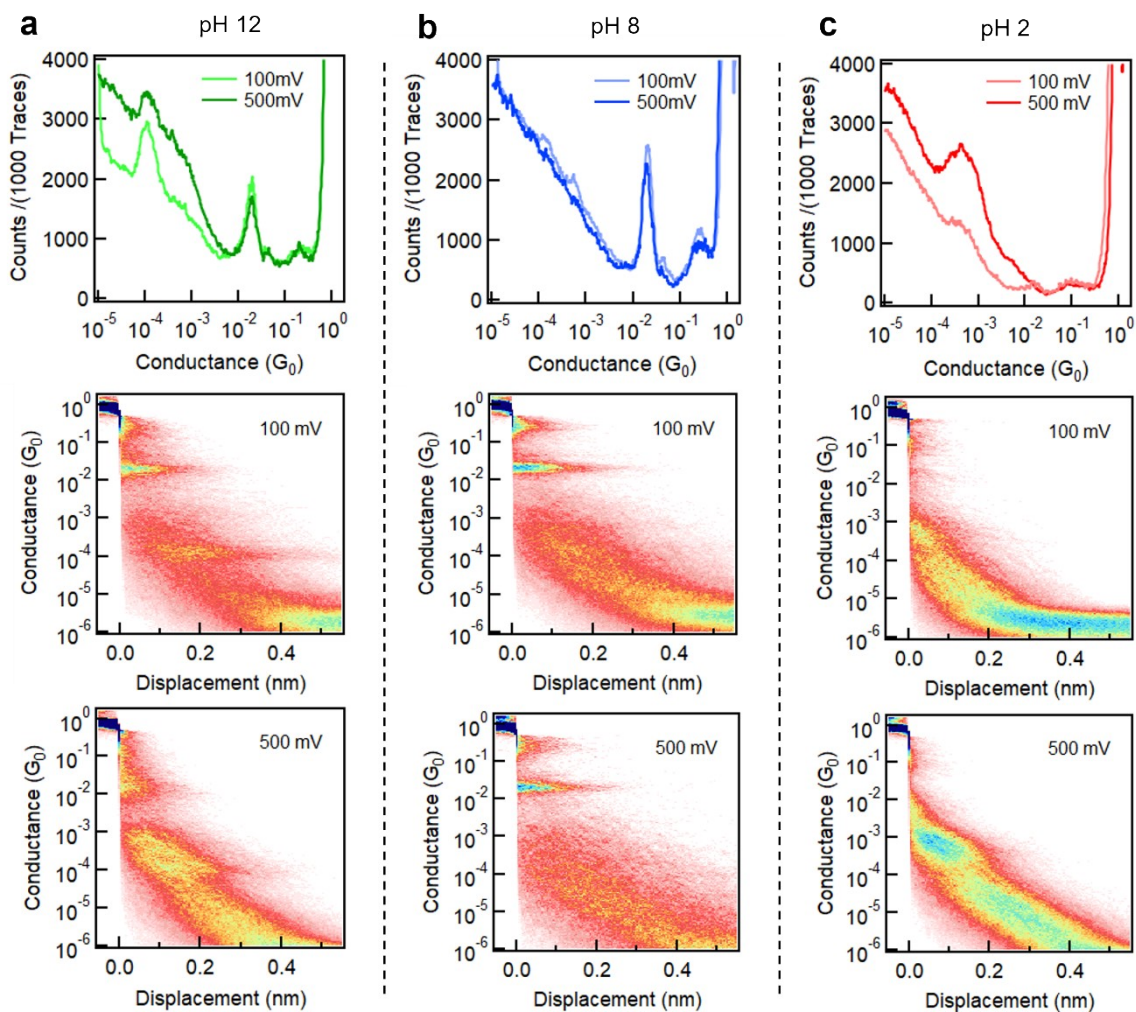


Figure S4. 1D and 2D conductance histograms of Tr123 measured out of various aqueous conditions: **(a)** pH 12, **(b)** pH 8, and **(c)** pH 2 with low ($V_{\text{bias}}=100$ mV) and high ($V_{\text{bias}}=500$ mV) applied voltages using the dip-coating method.

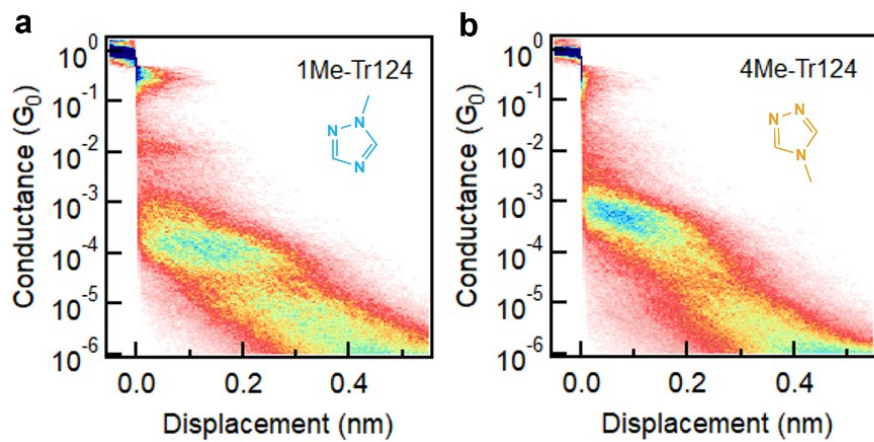


Figure S5. 2D conductance-displacement histograms of **(a)** 1Me-Tr124 and **(b)** 4Me-Tr124 (structures shown inset) measured in TCB ($V_{\text{bias}}=500$ mV).

3. Additional Calculation Data

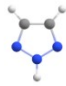

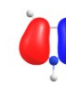
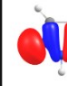
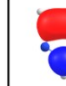
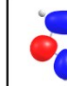
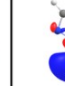
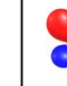

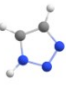

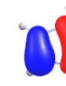

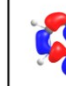
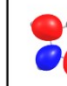



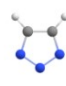



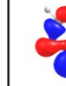
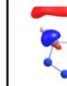
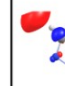
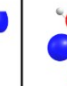

	HOMO-3	HOMO-2	HOMO-1	HOMO	LUMO	LUMO+1	LUMO+2	LUMO+3
								
2H-Tr123	-7.99 eV	-7.34 eV	-7.12 eV	-6.91 eV	-1.46 eV	-0.25 eV	-0.01 eV	0.42 eV
								
1H-Tr123	-7.94 eV	-7.62 eV	-6.68 eV	-6.39 eV	-1.39 eV	-0.57 eV	-0.14 eV	0.31 eV
								
Tr123 ⁻	-1.00 eV	-0.56 eV	-0.51 eV	-0.46 eV	3.92 eV	4.43 eV	5.13 eV	5.59 eV

Figure S6. Calculated frontier MOs of neutral (*1H*- and *2H*-) and anionic Tr123 in gas phase using FHI-aims with the PBE functional and ‘tight’ level basis set.

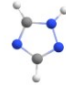

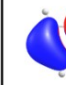
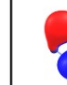
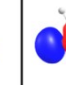


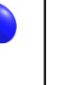
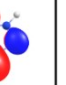

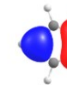
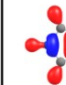
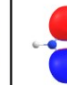
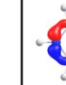


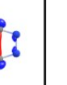
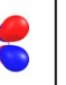
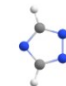

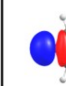




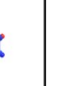
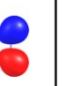
	HOMO-3	HOMO-2	HOMO-1	HOMO	LUMO	LUMO+1	LUMO+2	LUMO+3
								
1H-Tr124	-8.01 eV	-7.56 eV	-6.80 eV	-6.65 eV	-1.18 eV	-0.52 eV	-0.10 eV	0.56 eV
								
4H-Tr124	-7.69 eV	-7.49 eV	-6.69 eV	-6.00 eV	-0.94 eV	-0.80 eV	-0.38 eV	0.37 eV
								
Tr124 ⁻	-1.09 eV	-0.83 eV	-0.47 eV	-0.43 eV	4.21 eV	4.40 eV	5.36 eV	5.57 eV

Figure S7. Calculated frontier MOs of neutral (*1H*- and *4H*-) and anionic Tr124 in gas phase using FHI-aims with the PBE functional and ‘tight’ level basis set.

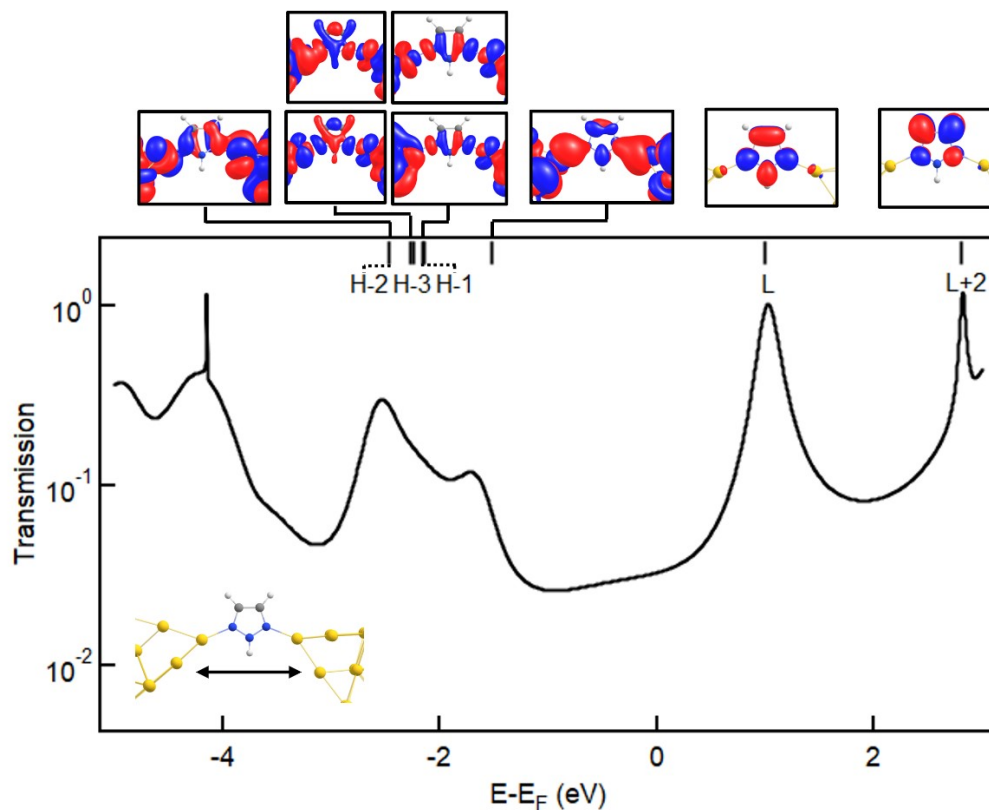


Figure S8. Isosurface plots of representative eigenchannels identified with gas-phase MOs of neutral Tr123 (*2H*-Tr123) (top) and corresponding eigenenergies plotted with the transmission spectrum (bottom). HOMO does not participate in transport near E_F , as no electron density is present in that orbital at the non-adjacent nitrogen atoms (N1 and N3) where binding occurs (**Figure S6**). The peak at ~ -1.5 eV cannot be assigned to any single MO. The arrow represents the direction of junction elongation.

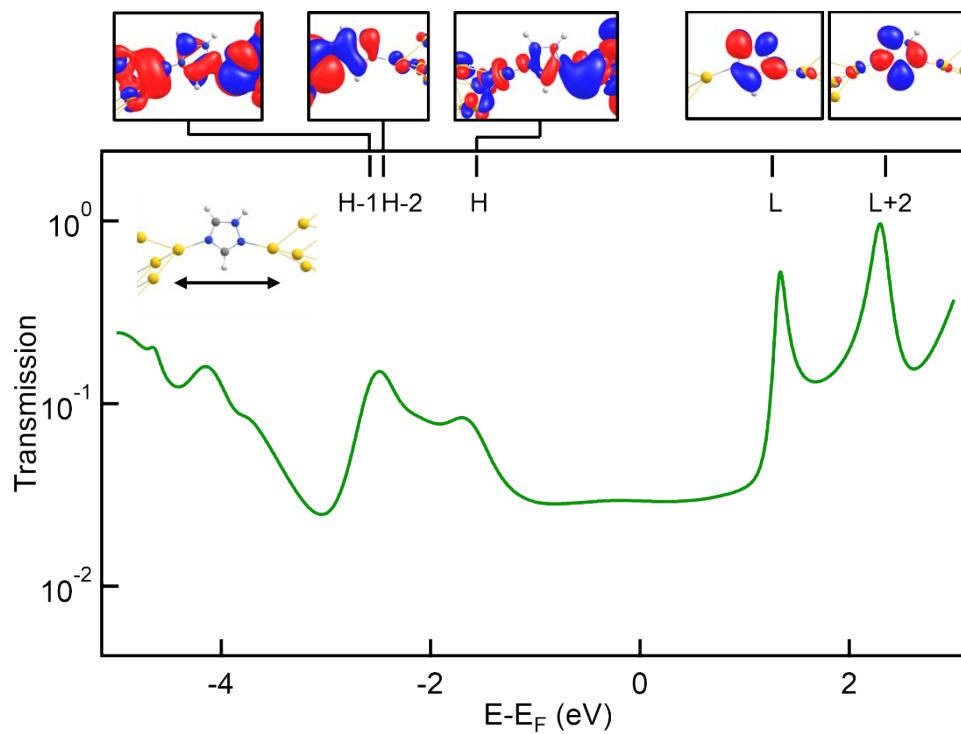


Figure S9. Isosurface plots of representative eigenchannels of neutral Tr124 (*IH*-Tr124) junctions (top) assigned to gas-phase MOs and the total transmission spectrum (bottom). The arrow represents the direction of junction elongation.

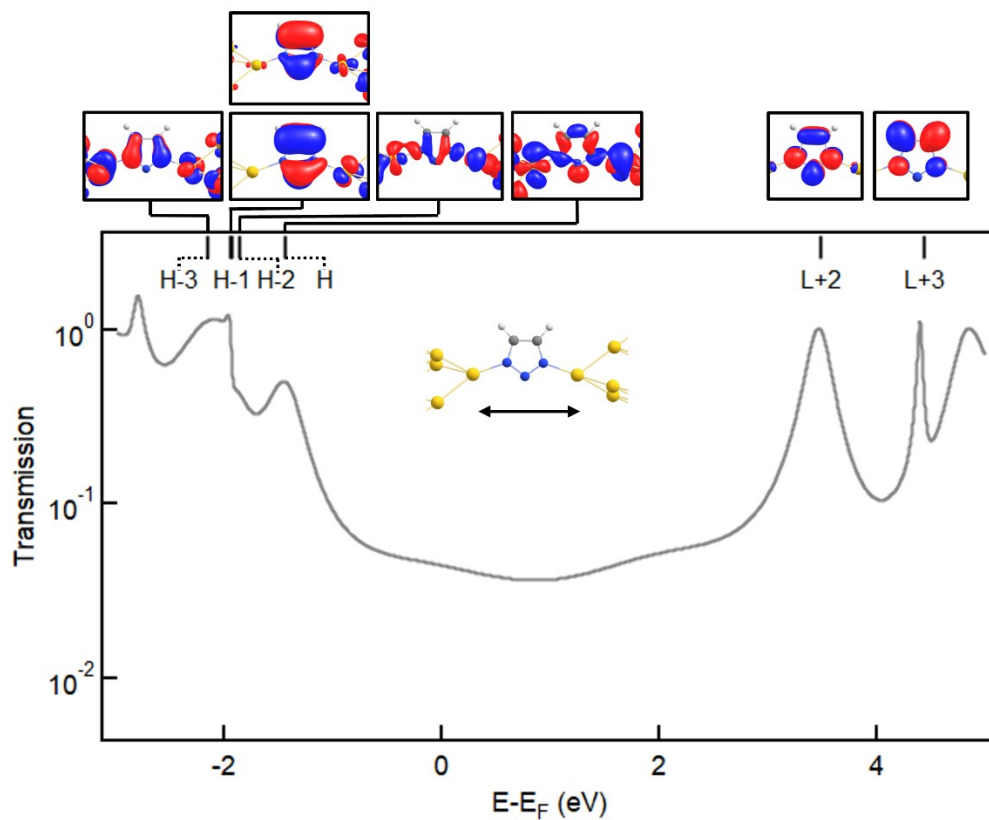


Figure S10. Isosurface plots of eigenchannels of anionic Tr123 junction (top) assigned to gas-phase MOs and the total transmission spectrum (bottom). The arrow represents the direction of junction elongation.

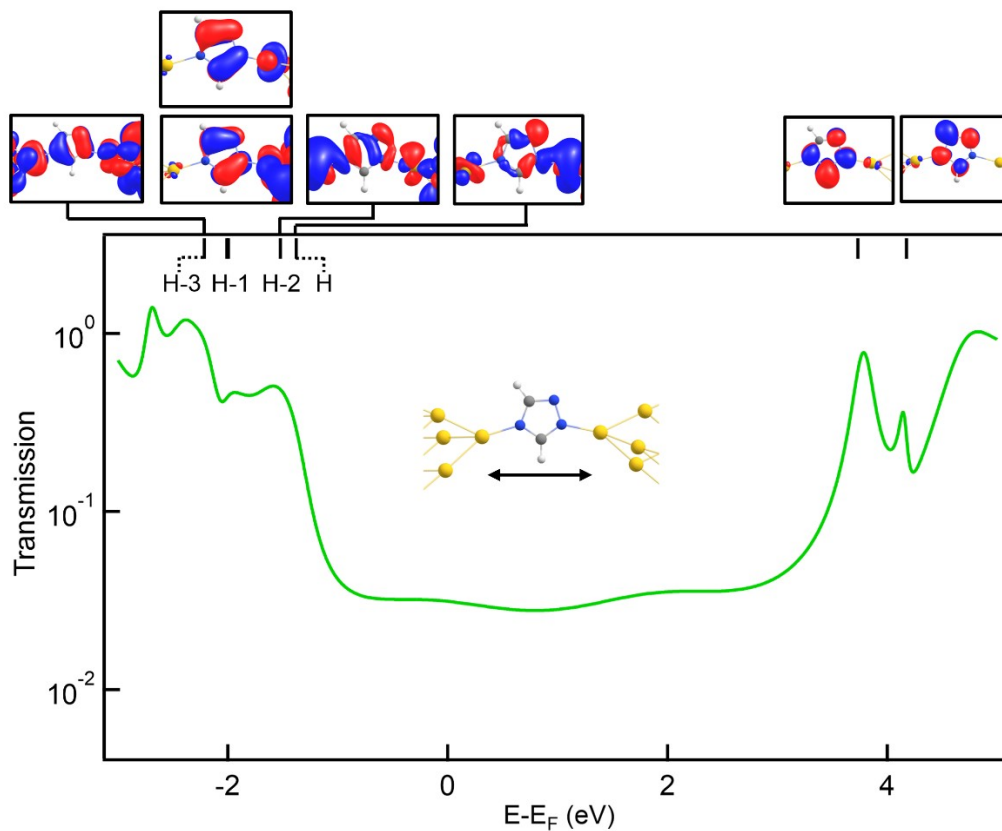


Figure S11. Isosurface plots of eigenchannels of anionic Tr124 junction (top) assigned to gas-phase MOs and the total transmission spectrum (bottom). The peaks at ~ 4 eV cannot be assigned to any single MO (e.g., LUMO+2 or LUMO+3) probably due to the charge redistribution when Tr124⁻ binds between electrodes. The arrow represents the direction of junction elongation.

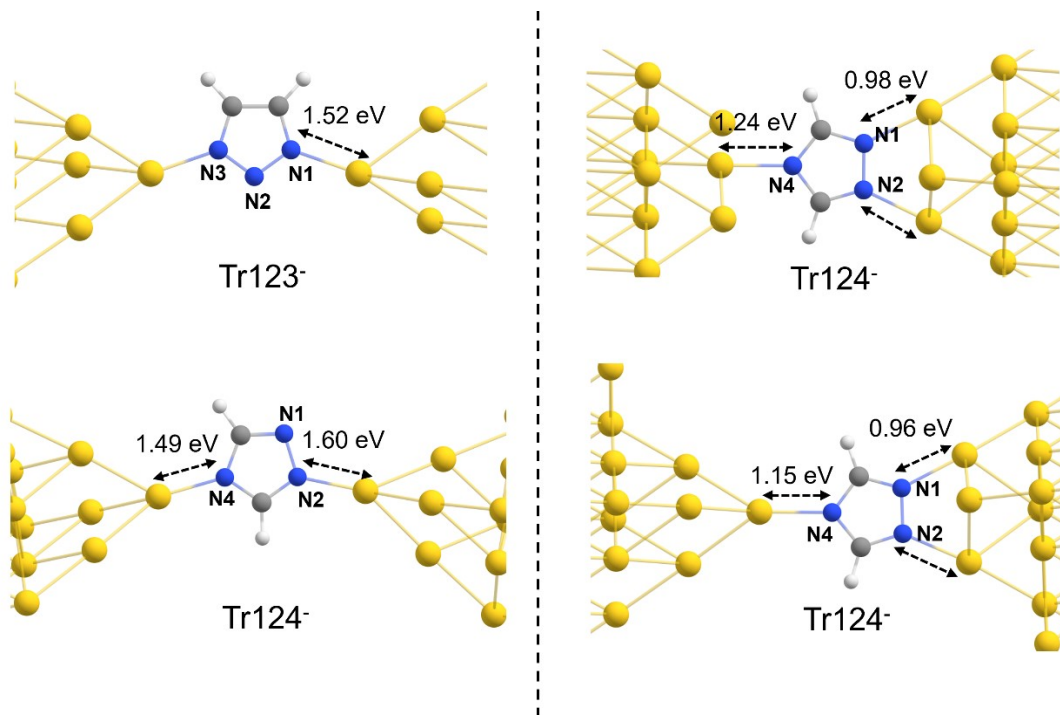


Figure S12. N-Au bond strength of Tr123⁻ and Tr124⁻ with two non-adjacent tertiary amine nitrogens binding to two sharp Au18 electrodes (left) and Tr124⁻ with all three nitrogens (N1, N2, and N4) binding to two dull Au21 electrodes (right, top) or one sharp Au22 and one dull Au21 electrode (right, bottom).

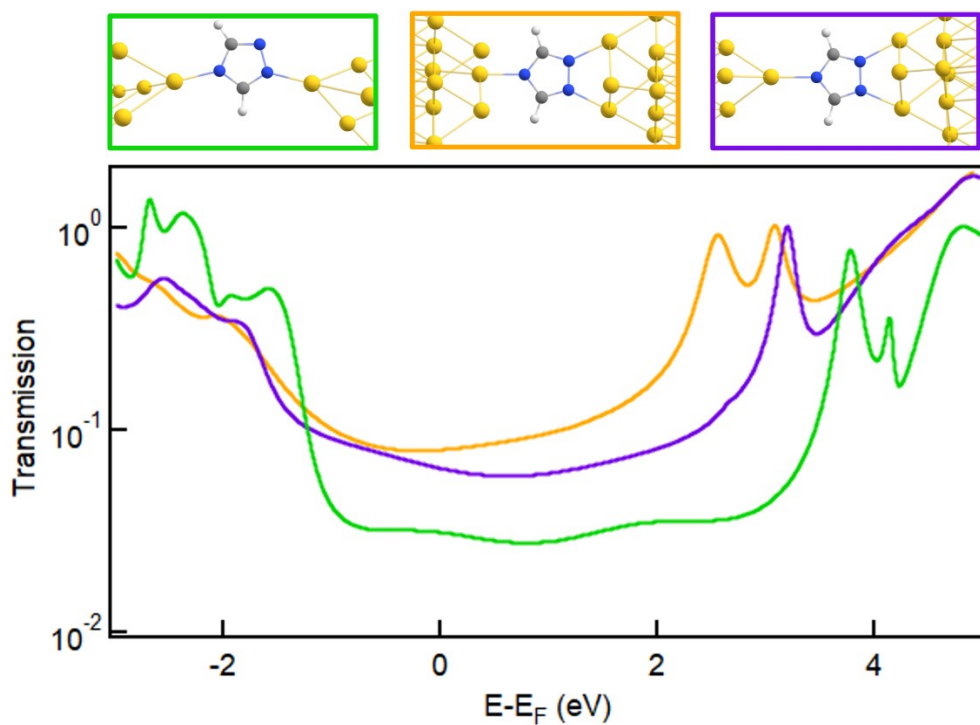


Figure S13. Various structures of Tr124⁻ bridging the junction (top) and the corresponding transmission spectra (bottom). Green shows single Tr124⁻ molecule bound to electrodes through non-adjacent tertiary amine nitrogens while orange and purple represent junctions with a third binding site as shown.

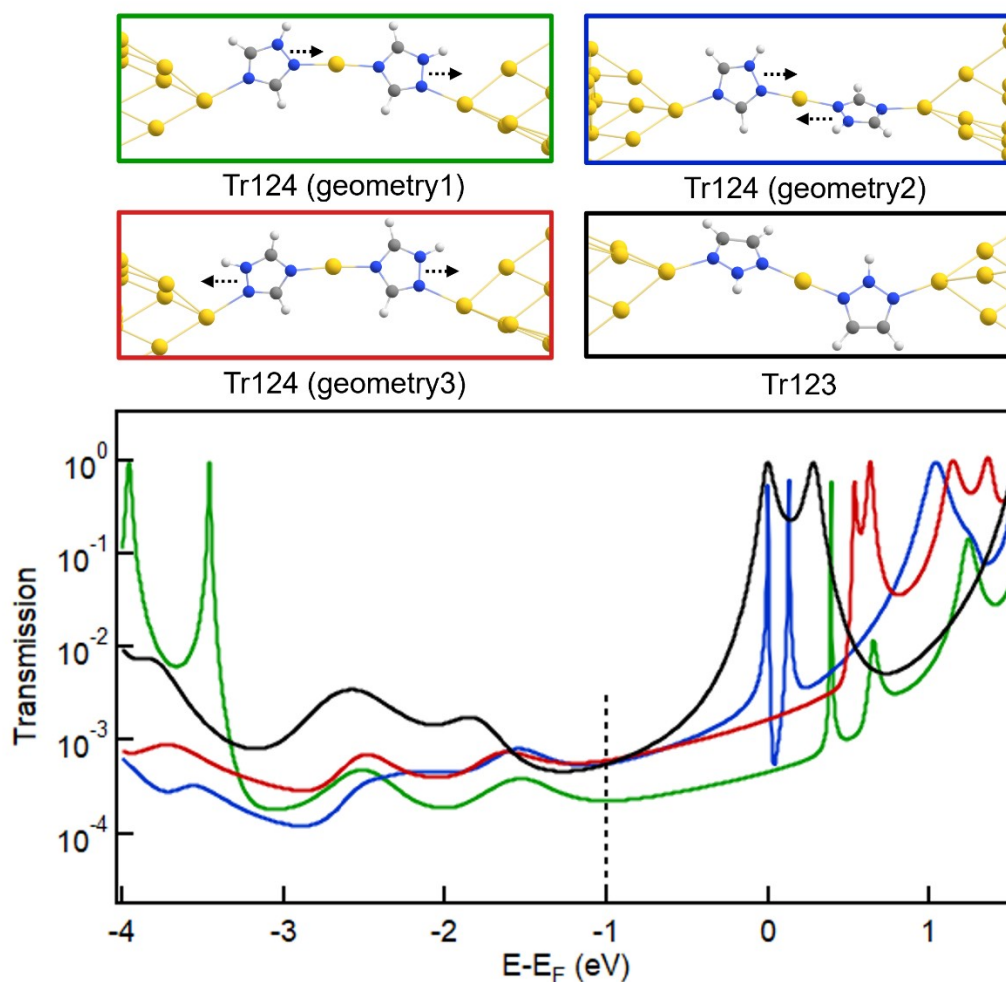


Figure S14. Various junction structures of neutral Tr123 and Tr124 chains with distinct arrangements of the nitrogen atoms with respect to the electrodes (indicated by the dashed arrows, top) and the corresponding transmission spectra (bottom). The number of electrons in the structure was adjusted to make the overall junction closed shell. In this case, the DFT calculations, which always underestimate the HOMO-LUMO gap and make errors in the prediction of MO alignments with the Fermi level, misplace the LUMO resonances too close to E_F . Based on experiment, the correct position of the Fermi energy is close to ~ -1 eV, as indicated by the vertical dashed line.

4. References

- (1) Venkataraman, L.; Klare, J. E.; Tam, I. W.; Nuckolls, C.; Hybertsen, M. S.; Steigerwald, M. L. Single-Molecule Circuits with Well-Defined Molecular Conductance. *Nano Lett.* **2006**, *6*, 458–462.
- (2) McNeely, J.; Miller, N.; Pan, X.; Lawson, B.; Kamenetska, M. Angstrom-Scale Ruler Using Single Molecule Conductance Signatures. *J. Phys. Chem. C* **2020**, *124*, 13427–13433.
- (3) Nagahara, L. A.; Thundat, T.; Lindsay, S. M. Preparation and Characterization of STM Tips for Electrochemical Studies. *Rev. Sci. Instrum.* **1989**, *60*, 3128–3130.
- (4) Capozzi, B.; Xia, J.; Adak, O.; Dell, E. J.; Liu, Z.-F.; Taylor, J. C.; Neaton, J. B.; Campos, L. M.; Venkataraman, L. Single-Molecule Diodes with High Rectification Ratios through Environmental Control. *Nat. Nanotechnol.* **2015**, *10*, 522–527.
- (5) Pan, X.; Qian, C.; Chow, A.; Wang, L.; Kamenetska, M. Atomically Precise Binding Conformations of Adenine and Its Variants on Gold Using Single Molecule Conductance Signatures. *J. Chem. Phys.* **2022**, *157*, No. 234201.
- (6) Pan, X.; Lawson, B.; Rustad, A. M.; Kamenetska, M. PH-Activated Single Molecule Conductance and Binding Mechanism of Imidazole on Gold. *Nano Lett.* **2020**, *20*, 4687–4692.
- (7) Skipper, H. E.; Lawson, B.; Pan, X.; Degtiareva, V.; Kamenetska, M. Manipulating Quantum Interference between σ and π Orbitals in Single-Molecule Junctions via Chemical Substitution and Environmental Control. *ACS Nano* **2023**, *17*, 16107–16114.
- (8) Arnold, A.; Weigend, F.; Evers, F. Quantum Chemistry Calculations for Molecules Coupled to Reservoirs: Formalism, Implementation, and Application to Benzenedithiol. *J. Chem. Phys.* **2007**, *126*, No. 174101.
- (9) Blum, V.; Gehrke, R.; Hanke, F.; Havu, P.; Havu, V.; Ren, X.; Reuter, K.; Scheffler, M. Ab Initio Molecular Simulations with Numeric Atom-Centered Orbitals. *Comput. Phys. Commun.* **2009**, *180*, 2175–2196.
- (10) Wilhelm, J.; Walz, M.; Stendel, M.; Bagrets, A.; Evers, F. Ab Initio Simulations of Scanning-Tunneling-Microscope Images with Embedding Techniques and Application to C₅₈-Dimers on Au(111). *Phys. Chem. Chem. Phys.* **2013**, *15*, 6684–6690.
- (11) Perdew, J. P.; Burke, K.; Ernzerhof, M. Generalized Gradient Approximation Made Simple. *Phys. Rev. Lett.* **1996**, *77*, 3865–3868.

- (12) Lawson, B.; Zahl, P.; Hybertsen, M. S.; Kamenetska, M. Formation and Evolution of Metallocene Single-Molecule Circuits with Direct Gold- π Links. *J. Am. Chem. Soc.* **2022**, *144*, 6504–6515.